Directional ordering in amorphous Co–Si–B alloys

2004 J. Phys.: Condens. Matter 16 3745

(http://iopscience.iop.org/0953-8984/16/21/023)

INSTITUTE OF PHYSICS PUBLISHING JOURNAL OF PHYSICS: CONDENSED MATTER

J. Phys.: Condens. Matter **16** (2004) 3745–3760 PII: S0953-8984(04)76012-9

Directional ordering in amorphous Co–Si–B alloys

R Andrejco and P Vojtanik[1]

Institute of Physics, Faculty of Science, P J Šafárik University, Park Angelinum 9, 041 54 Košice, Slovakia

E-mail: vojtanik@kosice.upjs.sk

Received 6 February 2004
Published 14 May 2004
Online at stacks.iop.org/JPhysCM/16/3745
DOI: 10.1088/0953-8984/16/21/023

Abstract

Directional ordering in the amorphous $Co_{75}Si_{15}B_{10}$ alloys by means of the magnetic after-effect (MAE) of the initial reluctivity and its influence on the Perminvar effect have been investigated. Two peak MAE spectra were obtained from isochronal measurements for as-cast as well as annealed samples. The spectrum of the as-cast sample has peak maxima at 383 and 545 K. Comparing this MAE spectrum with the spectrum of amorphous $Co_{75}B_{25}$ alloy, we identified the first peak as a result of Co–B atom pair reorientation (B-type relaxation) and the second one at higher temperatures as a result of Co–Si atom pair reorientation (Si-type relaxation). After annealing, the peaks shift to 442 and 576 K, respectively. For the numerical analysis of $Co_{75}Si_{15}B_{10}$ MAE spectra we modified the micromagnetic model assuming the existence of more relaxation processes, where each process is connected to the relaxation of one metalloid element. The pre-exponential factor for B-type relaxation was found to be $\tau_{0,AC}^{(B)} = 7 \times 10^{-17}$ s with the most probable activation energy $Q_{AC}^{*(B)} = 1.31$ eV. These values correlate very well with the magnetic relaxation (MR) activation parameters of $Co_{75}B_{25}$ alloy, $\tau_{0,AC} = 2 \times 10^{-17}$ s and $Q_{AC}^{*} = 1.35$ eV. Si-type relaxation has activation parameters $\tau_{0,AC}^{(Si)} = 6 \times 10^{-18}$ s and $Q_{AC}^{*(Si)} = 1.96$ eV. After annealing the sample at 683 K for 30 min they change to values $\tau_{0,AN}^{(B)} = 2 \times 10^{-15}$ s, $Q_{AN}^{*(B)} = 1.38$ eV and $\tau_{0,AN}^{(Si)} = 3 \times 10^{-17}$ s, $Q_{AN}^{*(Si)} = 2.01$ eV. The complicated shapes of the long-time isotherms reflect the superposition of two relaxation processes. We have numerically split each isotherm into two sub-isotherms representing the particular contributions of the two relaxation processes. The MAE spectrum of the critical field measured on the as-cast sample also has two peaks, like the reluctivity spectrum. The impact of Co–B and Co–Si atom pairs on the behaviour of the domain wall stabilization potential is discussed for the explanation of the observed MR results.

[1] Author to whom any correspondence should be addressed.

Introduction

A typical magnetic after-effect (MAE) spectrum of an amorphous ferromagnet can be divided in three characteristic temperature regions [1]. The first region is situated in temperatures well below room temperature, where the spectrum is nearly temperature independent. The second region is characterized by one broad intensive peak, originating from thermally activated relaxation processes. The last region can be found just below the Curie temperature. A peak can be found here, too, but the features of this peak are different from that of the second region. The peak just below the Curie temperature is usually narrow, and originates from a ferromagnetic to paramagnetic phase transition. This description of a typical MAE spectrum holds for a wide variety of compositions, from binary (Co, Fe)-M, where M is a metalloid [2–5] through ternary and quaternary alloys [1, 6–8] to multicomponent systems [9]; hence some authors argue (see [10] and references therein) that the magnetic relaxation has a structural, rather than compositional nature.

A special group of MAE spectra are those composed of more than one broad peak. Two peaks appear in ternary $Fe_{20}Ni_{60}B_{20}$ [1] and the Fe–Co–Zr system [11], but multi-peak MAE spectra can be more frequently found in multicomponent alloys [12–17]. The features of these peaks and their positions well under the Curie temperature indicate that they originate from thermally activated processes. The spectra of activation energies obtained from these MAE spectra also have more peaks. Three-peak spectra of activation energies were obtained from the analysis of isothermal measurements [18]; these were attributed to the presence of different relaxation processes.

There are too few papers investigating the connection between the compositions of amorphous alloys and their MAE spectra [1, 4]. In this paper we present our analysis of the two-peak MAE spectra of the amorphous $Co_{75}Si_{15}B_{10}$ alloy. For these purposes we extended the micromagnetic model of the MAE [19–21] and applied it for the analysis of the MAE spectra of as-cast and annealed alloys, which have two clearly separated peaks, both being broad and situated well below the Curie temperature. The novelty of this approach is in the transition from the magnetic relaxation originating from the directional reordering of anonymous atom pairs to the directional reordering of concrete atom pairs.

Structural magnetic relaxation appears in all amorphous transition-metal-based alloys with metalloid alloying. This phenomenon significantly influences their processibility, and magnetic as well as structural stability; hence it is important to understand the directional ordering in these alloys.

1. Model presentation

1.1. Basic assumptions

The concept of magnetic relaxation in amorphous alloys is similar to that of crystalline materials. Relaxation phenomena are in both cases related to reorientations of anisotropic point defects and their clusters, which interact with local magnetization in accordance with the principle of free energy minimization. Reorientations of atom pairs around vacancies in crystalline materials affect the time as well as temperature dependence of the initial reluctivity ($r = 1/\chi$, where χ is the susceptibility). The mobility of atom pairs in amorphous material is enabled by the presence of free volumes. In a simple model it is assumed that in the vicinity of the free volume these atom pairs may occupy two different orientations of their axes (figure 1(a)). The two orientations are separated by an energy barrier, which may be overcome either by thermal activation or by a tunnelling process. Such a transition can be

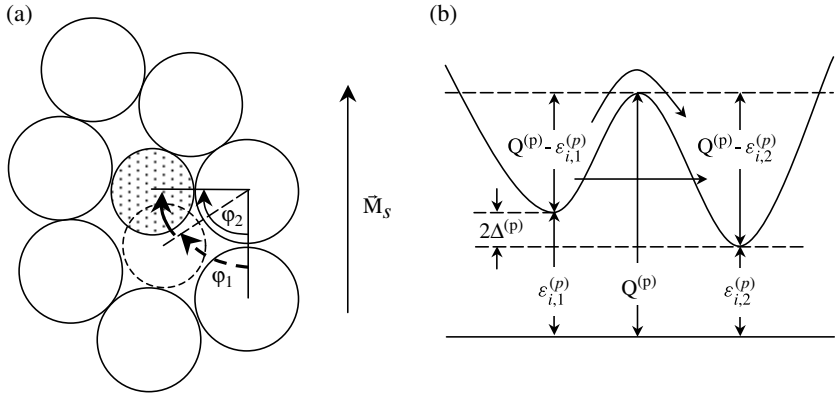

Figure 1. (a) Reorientation of the atom pair axis during structural magnetic relaxation minimizing the free energy of the system. $\vec{M}_S$: local magnetization; φ_1: initial angle; φ_2: final angle. (b) A two-level system for the local rearrangement of a mobile atom pair by thermal activation or a tunnelling process. $2\Delta^{(p)}$ is the splitting energy, $Q^{(p)}$ is the activation energy for transition, and $\varepsilon^{(p)}_{i,1}$ and $\varepsilon^{(p)}_{i,2}$ are the magnetic interaction energies in two pair axis orientations. The index p refers to the type of atom pairs.

schematically illustrated by a double-well model (figure 1(b)), which presents the situation from an energetic point of view.

If we assume a ternary alloy TM_1M_2, composed of transition ferromagnetic element T and two metalloids M_k, $k = 1, 2$, three types of atom pairs can be found in the vicinity of the free volume (T–T, T–M_1, and T–M_2). Pairs M_k–M_l, $k, l = 1, 2$, can be omitted, because there is very small probability for two metalloid atoms occupying nearest-neighbour positions.

Generally, when an alloy consists of P different types of atom pairs, it is convenient to introduce P different two-level systems (TLSs), each with parameters related to its own type of atom pair. Differences in two-level systems are partly caused by different magnetic interaction energies between the pth atom pair type and the local magnetization

$$\varepsilon^{(p)}_{i,j} = \varepsilon^{(p)\mathrm{ex}}_{i,j} + \varepsilon^{(p)K}_{i,j} + \varepsilon^{(p)\mathrm{el}}_{i,j}, \qquad i = 1, \ldots, n^{(p)}_0, \quad j = 1, 2, \tag{1}$$

where $p = 1, \ldots, P$, $n^{(p)}_0$ is the number of atom pairs of the pth type in the unit volume able to relax and $\varepsilon^{(p)\mathrm{ex}}_{i,j}$, $\varepsilon^{(p)K}_{i,j}$, and $\varepsilon^{(p)\mathrm{el}}_{i,j}$ are the exchange, anisotropy and magnetoelastic energies of the pth atom pair type. The exchange energy depends on the spins carried by the atom pair; hence the chemical composition has a great impact on the exchange integrals. The magnetoelastic energy is connected with the saturated magnetostriction constant λ_S. This quantity can be simply measured and, as found experimentally, Co–B alloys have negative λ_S as opposed to the positive λ_S of Fe–B alloys [22]. This indicates a significant influence of the alloy's chemical composition on magnetoelastic interactions in the sample. The anisotropy energy also depends on the amorphous alloy chemistry, as has been shown in [22, 23].

The splitting energy $2\Delta^{(p)}$ is composed of a structural term, $2\Delta^{(p)}_S$, and a magnetic term, $2\Delta^{(p)}_M$. When reorientations are driven by magnetic interactions, the splitting energy changes predominantly via the magnetic term, which for the ith atom pair is

$$2\Delta^{(p)}_{M,i} = \varepsilon^{(p)}_{i,2} - \varepsilon^{(p)}_{i,1}. \tag{2}$$

We deal with P groups of atom pairs. The atom pair in each group has its own parameters describing the TLS, the splitting energy $2\Delta^{(p)}_M$, the magnetic interaction energy $\varepsilon^{(p)}_{i,j}$ and the activation energy $Q^{(p)}_i$. Looking at one group of pairs, we can find distributions in these

parameters. For a simpler description of whole group, it is useful to introduce mean values of the characteristic parameters, $2\Delta_{\mathrm{M}}^{(p)}$, $Q^{(p)}$ and $\varepsilon_{\mathrm{eff}}^{(p)}$.

1.2. The kinetics of the transitions

In order to describe the time dependence of the transitions between two states of pair axis orientations, let us denote $n_j^{(p)}$ as the number of occupied states with orientations $j = 1, 2$ in the group of pth atom pair type in the unit volume of the alloy. The set of equations (3) describes the redistributions of the TLSs.

$$\mathrm{d}n_j^{(p)}/\mathrm{d}t = -\nu_{jj'}^{(p)} n_j^{(p)} + \nu_{jj'}^{(p)} n_{j'}^{(p)}, \qquad p = 1, \ldots, P, \quad j \neq j', \quad j, j' = 1, 2. \tag{3}$$

$\nu_{jj'}^{(p)}$ are the jump frequencies for the pth atom pair type transition between orientations j and j'. They can be expressed as

$$\nu_{jj'}^{(p)} = \nu_{00} \mathrm{e}^{S_{jj'}^{(p)}/k} \mathrm{e}^{-(Q^{(p)} - \varepsilon_{jj'}^{(p)})/kT}. \tag{4}$$

Here ν_{00} denotes an attempt frequency of the order of the Debye frequency, $S_{jj'}^{(p)}$ is the activation entropy for transition $j \to j'$, k is Boltzmann's constant and T is the absolute temperature. Assuming $\varepsilon_{jj'}^{(p)} \ll Q^{(p)}$ and $S_{jj'}^{(p)} = S_{j'j}^{(p)} = S^{(p)}$, which hold in the case of two nearly equivalent configurations, we can write

$$\nu_{jj'}^{(p)} \equiv \nu_{\mathrm{R}}^{(p)} = \nu_0^{(p)} \mathrm{e}^{-Q^{(p)}/kT}, \tag{5}$$

where the term $\nu_{00} \exp(S^{(p)}/k)$ has been replaced by the pre-exponential factor $\nu_0^{(p)}$. The index R in $\nu_{\mathrm{R}}^{(p)}$ indicates reversibility between the transitions in the TLS. Instead of $\nu_{\mathrm{R}}^{(p)}$, the parameter $\tau_{\mathrm{R}}^{(p)}$, where $\tau_{\mathrm{R}}^{(p)} = 1/\nu_{\mathrm{R}}^{(p)}$, is frequently used. $\tau_{\mathrm{R}}^{(p)}$ is a further important parameter related to pth atom pair type reorientation.

The solution of equations (3) can be simplified with the assumptions that in each group of atom pairs with the same chemical composition only one type of TLS with splitting energy $2\Delta^{(p)}$ exists, the TLSs are uncoupled, and at time $t = 0$ the initial condition $n_1^{(p)}(0)/2 = n_2^{(p)}(0)/2 = n_0^{(p)}/2$ holds. Equation (6) is the solution of (3) for the pth atom pair type:

$$n_j^{(p)}(\Delta^{(p)}, t) = \frac{n_0^{(p)}}{2}\left[1 - (-1)^j \tanh\frac{\Delta^{(p)}}{kT}(1 - \mathrm{e}^{-t/\tau_{\mathrm{R}}^{(p)}})\right], \qquad j = 1, 2. \tag{6}$$

Equation (6) describes only reversible transitions. Equations (3) can be expanded by introducing annealing jump frequencies $\nu_{\mathrm{A}}^{(p)}$ if the total number of TLSs decreases due to annealing. In that case $n_0^{(p)}$ in (6) has to be replaced by the expression

$$n_0^{(p)}(t) = n_\infty^{(p)} + [n_0^{(p)}(0) - n_\infty^{(p)}]\mathrm{e}^{-t/\tau_{\mathrm{A}}^{(p)}} \tag{7}$$

where $\tau_{\mathrm{A}}^{(p)} = 1/\nu_{\mathrm{A}}^{(p)}$ and $n_\infty^{(p)}$ is the equilibrium number of atom pairs of pth type at temperature T.

1.3. The stabilization potential of the domain wall and time dependence of the MAE

The determination of the stabilization potential of the domain wall (DW) interacting with defects is important for expressing the change of the reluctivity with time. The stabilization potential of the DW is defined as

$$\varphi_{\mathrm{S}} = \sum_{p=1}^{P} \sum_{i=1}^{n_0^{(p)}} \sum_{j=1,2} [n_j^{(p)}(z_i, t) - n_{j,0}^{(p)}]\varepsilon_{i,j}^{(p)}(z_i), \tag{8}$$

where $n_j^{(p)}(z_i, t)$ is the volume concentration of the mobile defects with orientation j in position z_i at time t after demagnetization and $n_{j,0}^{(p)}$ is the concentration at time $t = 0$. $\varepsilon_{i,j}^{(p)}$ is defined by (1).

MAE measurements are usually performed in small driving fields, which displaces the DW a distance U from its original position. The stabilization potential is then determined by the defect concentrations $n_j^{(p)}(z_i, t)$ and new interaction energies $\varepsilon_{i,j}^{(p)}(z_i - U)$. Replacing the summation over i by integration over z, the stabilization potential per unit DW area may be written as

$$\varphi_S = -\sum_{p=1}^{P} n_0^{(p)}(1 - e^{-t/\tau^{(p)}}) \int_{-\infty}^{-\infty} \left\langle \Delta^{(p)}(z - U) \tanh \frac{\Delta^{(p)}(z)}{kT} \right\rangle dz. \tag{9}$$

The integral from the previous equation can be transformed to a simpler form; see [20]. The change of the reluctivity with time can finally be expressed as

$$\begin{aligned} \Delta r(t) = \frac{1}{\chi(t)} - \frac{1}{\chi(0)} &= \frac{1}{2SM_S^2} \frac{d^2\varphi_S(U,t)}{dU^2} \\ &= \frac{2}{15S\delta_0 M_S^2} \sum_{p=1}^{P} n_0^{(p)}(t) \frac{\langle(\varepsilon_{\text{eff}}^{(p)})^2\rangle}{kT} \left\langle \frac{1}{\cosh^2(\Delta_S^{(p)}/kT)} \right\rangle (1 - e^{-t/\tau^{(p)}}). \end{aligned} \tag{10}$$

S denotes the DW area per unit volume, δ_0 is the DW thickness, M_S the saturation magnetization, and the effective interaction constant $\langle(\varepsilon_{\text{eff}}^{(p)})^2\rangle$ is defined as

$$\langle(\varepsilon_{\text{eff}}^{(p)})^2\rangle = \langle(\varepsilon^{(p)\text{ex}})^2\rangle + \langle(\varepsilon^{(p)K})^2\rangle + \langle(\varepsilon^{(p)\text{el}})^2\rangle. \tag{11}$$

One can substitute expressions (7)–(10) instead of $n_0^{(p)}(t)$, and also general relaxation functions G_R and G_A may be introduced to obtain a more general equation. This gives

$$\Delta r(t) = \frac{2}{15S\delta_0 M_S^2} \sum_{p=1}^{P} \frac{\langle(\varepsilon_{\text{eff}}^{(p)})^2\rangle}{kT} \left\langle \frac{1}{\cosh^2(\Delta_S^{(p)}/kT)} \right\rangle [n_\infty^{(p)} G_R^{(p)}(t) + \Delta n^{(p)} G_R^{(p)}(t) G_A^{(p)}(t)] \tag{12}$$

where

$$G_R^{(p)} = \int P_R^{(p)}(\tau_R^{(p)})(1 - e^{t/\tau_R^{(p)}})\, d\tau_R^{(p)} \tag{13a}$$

$$G_A^{(p)} = \int P_A^{(p)}(\tau_A^{(p)}) e^{t/\tau_A^{(p)}}\, d\tau_A^{(p)} \tag{13b}$$

and $\Delta n^{(p)} = n_0^{(p)}(0) - n_\infty^{(p)}$. $n_0^{(p)}$ is the density of mobile defects in the as-quenched state and $n_\infty^{(p)}$ is the equilibrium concentration of mobile atom pairs which remains stable at temperature T. P_R and P_A are distributions of relaxation times. Equation (12) enables us to analyse reversible as well as irreversible relaxations of atom pairs with different chemical compositions. For $P = 1$ it is identical to the original micromagnetic model expression [21].

1.4. The stabilization potential of the DW and the field dependence of susceptibility

Structural relaxation of two-level systems leads to the formation of a stabilization potential which influences the behaviour of the magnetic structure. In order to push the DW out from its potential well, an external field is required. A small magnetic field causes only a reversible movement of the wall on the bottom of its potential well. The field dependence of the susceptibility in the small field region is constant. Because $\chi^{-1} \approx d^2\varphi_S/dU^2 = \text{constant}$,

the potential well has a parabolic shape. When the external field exceeds some critical value, pinning the field of the wall, H_P, an irreversible jump of the DW takes place and the susceptibility steeply increases.

In a real material, a set of domain walls exists, each with its own H_P. To simplify the description of such a situation, the critical field H_{CR} is usually used. It is defined as the minimal pinning field. Experimentally it can be simply obtained from the $\chi(H)$ dependence as the point at which χ starts to rise. The value H_{CR} is connected with the steepness of the potential well by the equation

$$H_{CR} = \frac{1}{2SM_S \cos\phi_0} \frac{\mathrm{d}\varphi_S(U,t)}{\mathrm{d}U}\bigg|_{\max} = \frac{\text{constant}}{SM_S \cos\phi_0} \times \sum_{p=1}^{P} c_0^{(p)}(t) \frac{\langle(\varepsilon_{\text{eff}}^{(p)})^2\rangle}{kT} \left\langle \frac{1}{\cosh^2 \Delta_S^{(p)}/kT} \right\rangle (1 - \exp(-t/\tau^{(p)})), \tag{14}$$

where ϕ_0 is the angle between the external field and $\vec{M}_S$ in the domain. A general relaxation function can be introduced to (14), too.

1.5. Application of the model

In previous sections we have presented the model based on the assumption of independent magnetic relaxations of different atom pairs. In the reorientation processes, the pairs T–M_i predominantly contribute to the reorientation process, because the M atoms are light and sufficiently mobile compared to T atoms. Hence the alloy $Co_{75}Si_{15}B_{10}$ can be analysed with two pre-exponential factors, where $\tau_0^{(B)}$ describes the magnetic relaxation of Co–B pairs and $\tau_0^{(Si)}$ holds for Co–Si. The model presented here is applicable for alloys of the type $TM_1M_2 \cdots M_L$, where analysis can by made with L pre-exponential factors. An analysis of the magnetic relaxation of an alloy with two transition metals and two metalloids will be presented in another paper.

2. Experimental details

A sample of $Co_{75}Si_{15}B_{10}$ was prepared by the rapid quenching method. The amorphicity was checked by x-ray diffraction. The Curie temperature was obtained from measurement of the initial susceptibility temperature dependence. Two sets of samples were investigated, as-cast as well as annealed at 683 K for 30 min in an argon atmosphere. The MAE spectra and long-time isotherms were measured by an LC oscillator technique with measuring field less than 0.1 A m^{-1} and frequencies around 10 kHz. These measurements were twice repeated, always with a new sample. The relaxation intensity is represented as $\Delta r/r = [r(t) - r(1\text{s})]/r(1\text{s})$, where $t = 2, 3, 5, 10, 20, 30, 60, 90, 120$ and 180 s. The MAE spectra and isotherms were numerically analysed by a least-squares method with a model function of the type

$$r(t,T) = r_0(T) + \sum_{p=1}^{2} \sum_{i=1}^{n} \Delta r_i^{(p)} G_R^{(p)}(\tau_0^{(p)}, t, T), \tag{15}$$

where $\tau_0^{(p)} = 1/\nu_0^{(p)}$, $p = 1, 2$ and n is the number of boxes used to replace the continuous distribution of relaxation times. $\Delta r_i^{(p)}$ represents the relaxation intensity of the ith box in the pth relaxation process.

We have also investigated the after-effect of the critical field. The field dependence of the susceptibility after demagnetization and stabilization was measured by the induction method.

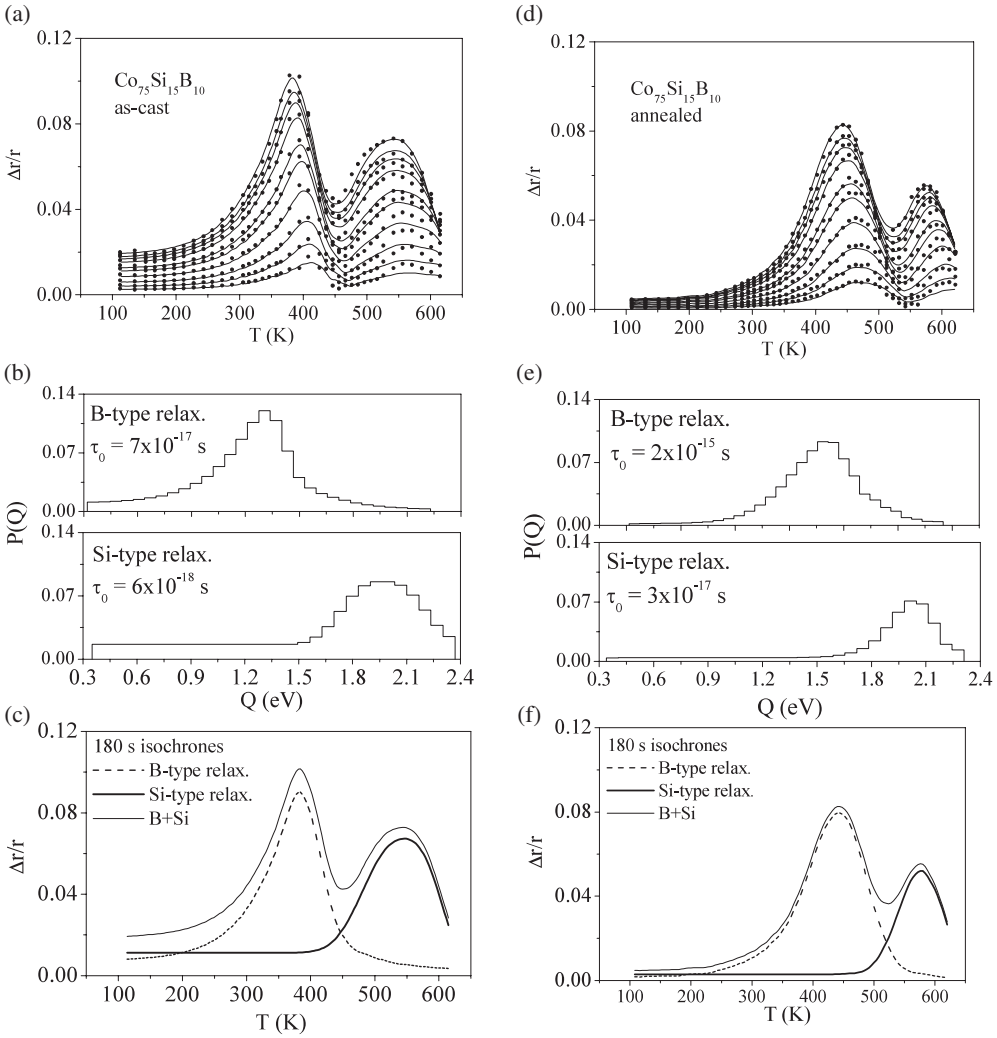

Figure 2. The MAE spectra of as-cast and annealed $Co_{75}Si_{15}B_{10}$ alloy ((a), (d)). Distributions of activation energies for B-type and Si-type relaxations ((b), (e)). 180 s isochrones for both relaxations and their superposition ((c), (f)).

3. Results and discussion

3.1. Isochronal measurements

The MAE spectrum of as-cast amorphous $Co_{75}Si_{15}B_{10}$ alloy consists of two peaks situated at 383 and 545 K with intensities 10.2% and 7.2% for time 180 s (figure 2(a)). Both peaks are well below the Curie temperature ($T_C = 663$ K). In order to investigate the relaxation of Co–B and Co–Si atom pairs in the $Co_{75}Si_{15}B_{10}$ sample, we have also measured the MAE spectrum of amorphous $Co_{75}B_{25}$ alloy. We found a single peak in its MAE spectrum, with maximum at 383 K and intensity 38% (figure 3(a)). Comparing these two spectra, we can conclude that substitution of B atoms by Si atoms reduces the MAE spectrum intensity from 38% to 10.2% without affecting its position, and causes the formation of the second relaxation

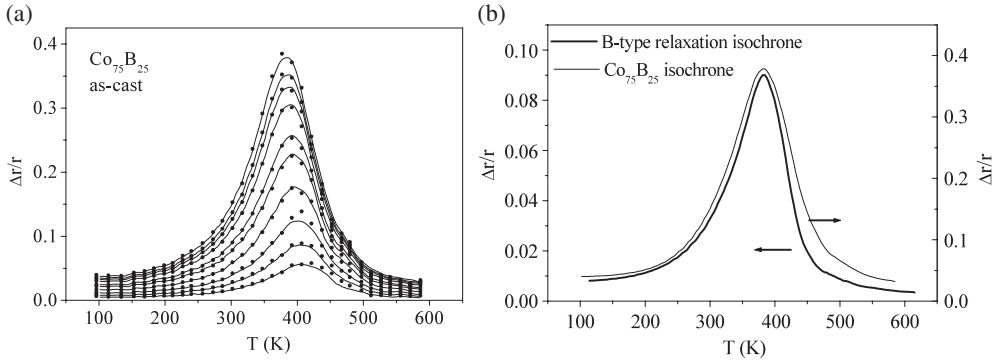

Figure 3. (a) The MAE spectrum of $Co_{75}B_{25}$. (b) A comparison between 180 s isochrones of B-type relaxation in as-cast $Co_{75}Si_{15}B_{10}$ and $Co_{75}B_{25}$ alloys.

peak at 545 K. The second relaxation peak in the $Co_{75}Si_{15}B_{10}$ MAE spectrum is connected to such a relaxation process, which is not present in the $Co_{75}B_{25}$ alloy. It cannot originate from a phase transition, because it is situated well below the Curie temperature, and is wide. Assuming that the relaxation in the $Co_{75}B_{25}$ alloy is realized by magnetic relaxation of Co–B atom pairs, we identified the first peak of the $Co_{75}Si_{15}B_{10}$ MAE spectrum as a result of Co–B pair relaxation (B-type MR) and the second one as originating from Co–Si pair relaxation (Si-type MR). Figure 3(b) compares 180 s isochrones of the B-type relaxation of the $Co_{75}B_{25}$ alloy with one obtained from numerical analysis of the $Co_{75}Si_{15}B_{10}$ alloy. Good qualitative agreement in their shapes proves our conclusions. The difference in relaxation intensities is because of the different amount of mobile defects in both samples.

Numerical analyses of the observed results were performed in two ways, first with a single pre-exponential factor and distribution of activation energies, then with two pre-exponential factors, where each factor has its own distribution of activation energies. We found the pre-exponential factor of Co–B pairs $\tau_{0,\mathrm{AC}}^{(\mathrm{B})} = 7 \times 10^{-17}$ s, which is in good agreement with τ_0 found from $Co_{75}B_{25}$ spectrum analysis ($\tau_{0,\mathrm{AC}} = 2 \times 10^{-17}$ s). This agreement in τ_0 indicates similar configurations around the Co–B atom pairs in both samples. Co–Si pairs have $\tau_{0,\mathrm{AC}}^{(\mathrm{Si})} = 6 \times 10^{-18}$ s. The order of τ_0 values in both cases indicates relaxation realized by atom pair axes reorientation. We found $\tau_{0,\mathrm{AC}}^{(\mathrm{B+Si})} = 3.1 \times 10^{-17}$ s when analysing the two-peak spectrum with only a single τ_0 value. This value lies between $\tau_{0,\mathrm{AC}}^{(\mathrm{B})}$ and $\tau_{0,\mathrm{AC}}^{(\mathrm{Si})}$. Such a result can be expected, because each group of relaxing atom pairs contributes to the mean τ_0 with some weight.

The differences in $\tau_{0,\mathrm{AC}}^{(\mathrm{B})}$ and $\tau_{0,\mathrm{AC}}^{(\mathrm{Si})}$ as well as in peak temperatures are reflected in the different most probable activation energies Q^*. We found $Q_{\mathrm{AC}}^{*(\mathrm{B})} = 1.31$ eV and $Q_{\mathrm{AC}}^{*(\mathrm{Si})} = 1.96$ eV; see figure 2(b). $Q_{\mathrm{AC}}^{*(\mathrm{B})}$ is very well comparable with the most probable activation energy of the $Co_{75}B_{25}$ alloy, $Q_{\mathrm{AC}}^{*} = 1.35$ eV. The higher $Q_{\mathrm{AC}}^{*(\mathrm{Si})}$ indicates lower mobility of Co–Si pairs. Higher activation energies of the Si-type MR can be explained not only by the larger dimensions of Si atoms but also by the strong chemical affinity between Si and Co atoms [24, 25].

It is interesting to compare the 180 s isochrones of B- and Si-type relaxations obtained from numerical analysis (figure 2(c)). At low temperatures both isochrones have constant values, and relaxation is realized by a tunnelling process. Si-type relaxation has a greater impact on the reluctivity change at low temperatures, possibly due to higher Si content. Increase of

temperature makes the thermal reorientation of Co–B atom pairs more intensive, as is indicated by the peak in the Co–B isochrone. In the temperature range where the most intensive B-type relaxation takes place, Si-type relaxation is still constant, and atom pair reorientation is realized by a tunnelling process even though these temperatures are high enough for B-type relaxation. Thermal activation of two-level systems in Si-type relaxation appears above 423 K.

We have also investigated the influence of annealing at $T_A = 683$ K on the behaviour of both type of MR. The MAE spectrum of the annealed sample again consists of two peaks, located at 442 K with intensity $\Delta r/r = 8.3\%$ and 576 K with $\Delta r/r = 5.6\%$ (figure 2(d)). Both peaks have reduced relaxation intensity and are shifted to higher temperatures, when compared to the as-cast alloy spectrum. Relaxation intensity reduction and shift of the peaks to higher temperatures are typical results of under-critical annealing. The first peak (442 K) can be associated with the MR of B-type and second one (576 K) with the MR of Si-type. After annealing, the Co–Si peak is shifted to higher temperatures by $\Delta T = 31$ K, which is a smaller change than the shift of the Co–B peak position, $\Delta T = 59$ K. The pre-exponential factor of Si-type relaxation is changed by one order after annealing, $\tau_{0,AN}^{(Si)} = 3 \times 10^{-17}$ s, as opposed to the two-order change of the B-type relaxation pre-exponential factor, $\tau_{0,AN}^{(B)} = 2 \times 10^{-15}$ s. When performing numerical analysis with single pre-exponential factors, we found $\tau_{0,AN}^{(B+Si)} = 4 \times 10^{-16}$ s. The pre-exponential factor is a structurally sensitive quantity. The changes in pre-exponential factors can be a measure of the changes in nearest-neighbourhoods of both atom pair types after annealing. Both pre-exponential factors are greater after annealing, hence structural configurations are closer to those present in crystalline material, which has τ_0 usually of the order 10^{-13} s [26]. The most probable activation energies are changed to values $Q_{AN}^{*(B)} = 1.38$ eV and $Q_{AN}^{*(Si)} = 2.01$ eV (see figure 2(e)).

Figure 2(f) presents 180 s isochrones of B-type and Si-type relaxations in the annealed sample. The isochrones have qualitatively similar behaviour as the isochrones of the as-cast sample (figure 2(e)).

3.2. Isothermal measurements

From isochronal measurements we have identified two relaxation processes with different activation parameters. For a more detailed study of these magnetic relaxation processes we measured long-time isotherms at suitable temperatures. As expected, the superposition of relaxation processes produced complicated shapes of isotherms.

According to measuring time and temperature, one can detect different stages of the magnetic relaxation process. Amorphous alloy relaxes with a wide distribution of relaxation times. This distribution can be characterized by the most probable relaxation time τ^*, which is temperature dependent and can be calculated by an Arrhenius equation $\tau^* = \tau_0 \exp(Q^*/kT)$. When (t_1, t_2) is the measuring time interval after demagnetization, three situations can occur according to the mutual relationship between τ^* and (t_1, t_2). At temperatures below the MAE peak $t_2 < \tau^*$, the isotherm reflects only the initial stages of relaxation. It has a convex shape in logarithmic scale. At temperatures around the relaxation peak, τ^* is reduced to values $t_1 < \tau^* < t_2$. The isotherm for time $t < \tau^*$ has a convex shape and for $\tau^* < t$ a concave one, with an inflexion point at time $t = \tau^*$. Further increase of temperature reduces τ^* to values lower than t_1, so the main part of the relaxation process takes place before the start of measurement and the isotherm has a concave shape.

For interpretation of the isotherm shapes measured for the $Co_{75}Si_{15}B_{10}$ alloy (see figures 4(a)–(k)), we introduced two τ^* values, $\tau^{*(B)}$ for B-type relaxation and $\tau^{*(Si)}$ for Si-type. We have split each measured isotherm into two sub-isotherms representing contributions

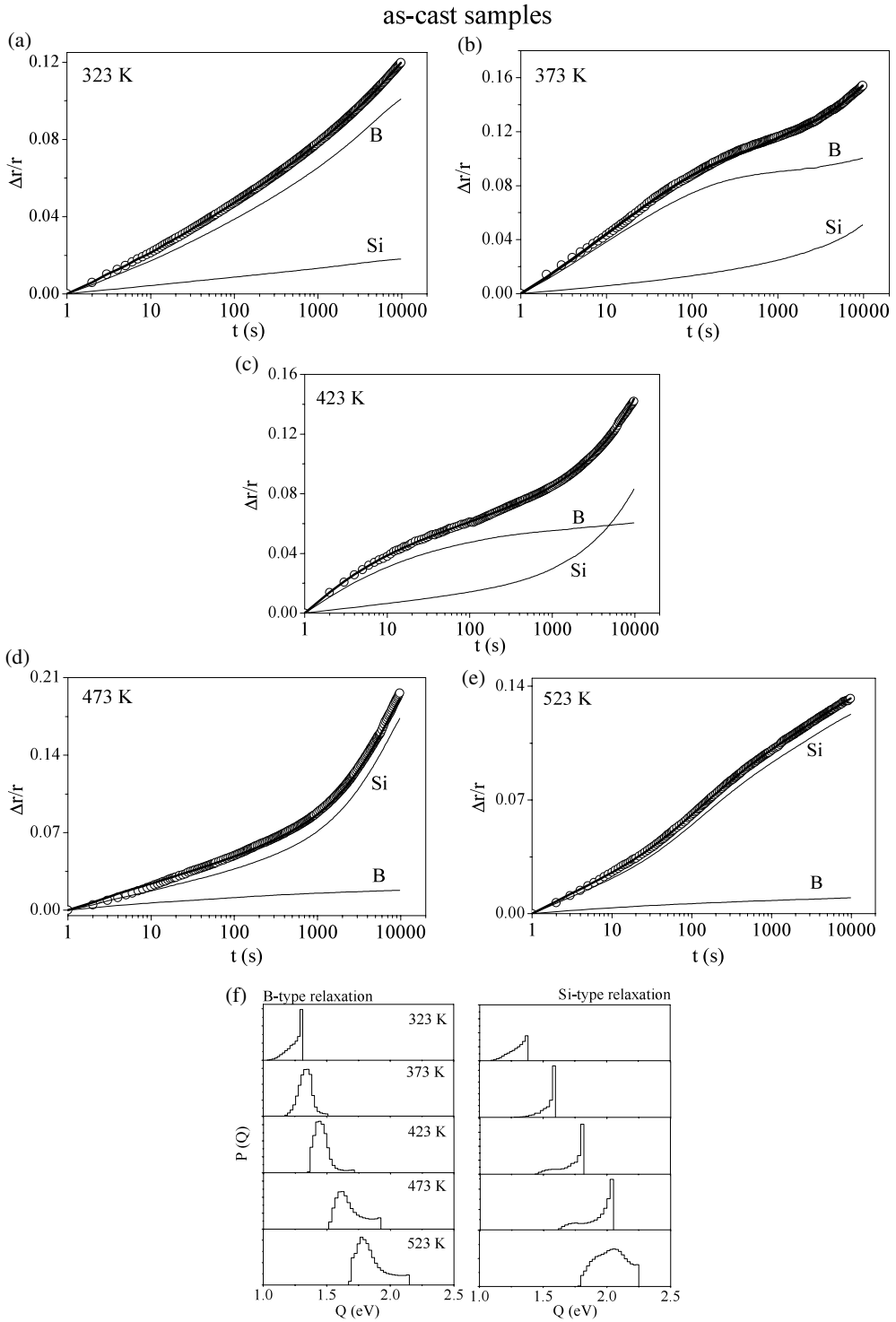

Figure 4. Isotherms of the magnetic after-effect measured at marked temperatures on as-cast ((a)–(e)) and annealed ((j)–(k)) samples. (B: B-type relaxation sub-isotherm; Si: Si-type relaxation sub-isotherm), (f) and (l): distributions of activation energies for particular relaxation processes.

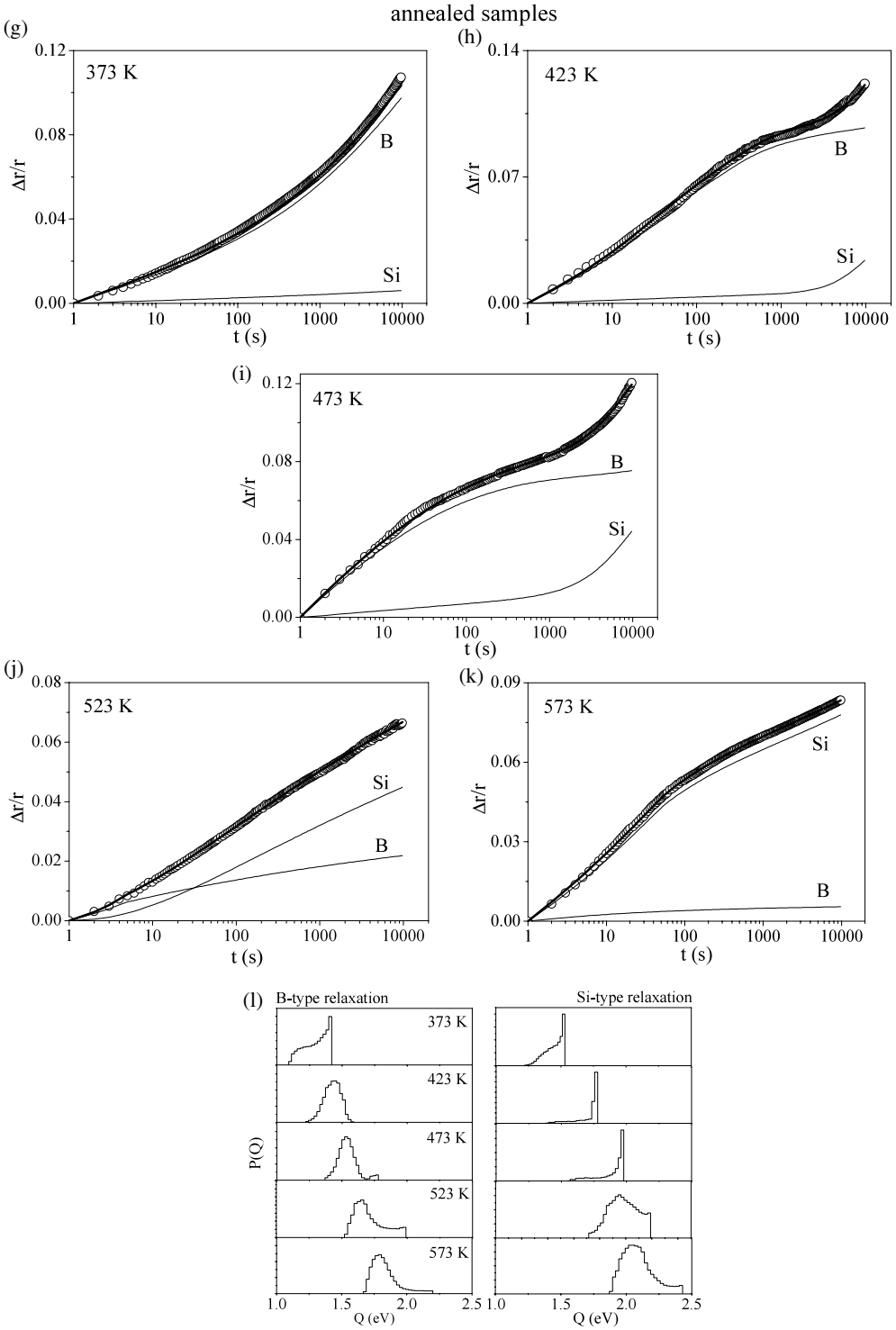

Figure 4. (Continued.)

of particular relaxation process. The isotherm measured at 323 K as well as its sub-isotherms have convex shapes (figure 4(a)). At 373 K (figure 4(b)), which is a temperature close to the B-type relaxation peak, the B-type relaxation sub-isotherm has an inflexion point at $t^* = 30$ s. The value calculated by the Arrhenius equation with $\tau_{0,\mathrm{AC}}^{(\mathrm{B})} = 7 \times 10^{-17}$ s and $Q_{\mathrm{AC}}^{*(\mathrm{B})} = 1.31$ eV, $\tau^{*(\mathrm{B})} = 35$ s, is very well comparable with the position of the inflexion point. At higher temperatures, the B-type relaxation sub-isotherms have only concave shape with decreasing relaxation amplitude at the end of the measurement, which describes saturation of this process (figures 4(c)–(e)). Si-type relaxation sub-isotherms have a convex shape up to 473 K (figures 4(a)–(d)). Inflexion points appear at 473 K at $t^* = 7900$ s, but one is visible more clearly at 523 K at $t^* = 135$ s (figure 4(e)). The positions of the inflexion points again well correspond to the theoretical value calculated with $\tau_{0,\mathrm{AC}}^{(\mathrm{Si})} = 6 \times 10^{-18}$ s and $Q_{\mathrm{AC}}^{*(\mathrm{Si})} = 1.96$ eV. Sub-isotherms of the relaxation processes of annealed samples (figures 4(g)–(k)) have qualitatively similar behaviour as those obtained from as-cast sample isotherms. B-type relaxation has an inflexion point 70 s after demagnetization at 423 K (figure 4(h)). Si-type relaxation has inflexion points at 523 K (figure 4(j)), $t^* = 370$ s, but more clearly visible is the one at 573 K (figure 4(k)), $t^* = 32$ s. These values are in good agreement with calculated $\tau^{*(\mathrm{Si})}$ values, when using $\tau_{0,\mathrm{AN}}^{(\mathrm{Si})} = 3 \times 10^{-17}$ s and $Q_{\mathrm{AN}}^{*(\mathrm{Si})} = 2.01$ eV. The shape of the activation energies spectrum (AES) depends on the shape of the sub-isotherm (figures 4(f), (l)). When the sub-isotherm has convex shape, the AES has a convex shape as well. Concave sub-isotherms have an AES with flat parts at higher activation energies. After annealing, values of activation energies covering relaxation processes are higher than for as-cast samples measured at same temperature. Annealing drastically alters the behaviour of two-level systems. The potential barrier separating the two orientations of the pair axis increases, because part of the free volume is reduced and part is completely annealed out. An atom pair in the vicinity of a smaller free volume requires higher activation energy for reorientation than the same pair for the same reorientation in the vicinity of a large free volume.

3.3. The Perminvar effect

Measurements of susceptibility-field dependences after demagnetization with different stabilization times enable us to investigate the development of the steepness of the potential wells. The steeper the well, the higher the H_{CR} value obtained, according to equation (14). The $\chi(H)$ dependence measured on an amorphous ferromagnet has three characteristic parts: a region with susceptibility constant up to critical field H_{CR} (defined as a lowest DW pinning field, H_{P}); a region with a steep increase between H_{CR} and H_{MAX}, where H_{MAX} is the field in which χ reaches its maximum value; and finally a part with decreasing χ at fields $H > H_{\mathrm{MAX}}$. These parts reflect different magnetization processes taking place during measurement. The part with constant χ is characterized by reversible movements of domain walls within their potential wells. Irreversible jumping of the DWs out from their potential wells causes the increase of χ, and its decrease is mainly given by the magnetization rotation at higher fields. The behaviour of χ at low fields reflects the time–temperature evolution of the potential well bottom. The reversible movement of the DW in the potential well can be described by the equation [27]

$$\vec{H} \cdot (\vec{I}_1 - \vec{I}_2) + P_{\mathrm{R}}(U) + P_{\mathrm{N}}(U, t) = 0. \tag{16}$$

Equation (16) expresses the equilibrium of the forces acting on a unit area of the wall. Here $\vec{H}$ is the external field and $\vec{I}_1$, $\vec{I}_2$ are the magnetizations in domains separated by the wall, P_{R} is the restoring pressure, which keeps the wall in the equilibrium position on the bottom of the Rayleigh potential well E_{R}, and P_{N} is the stabilization pressure as a result of development of

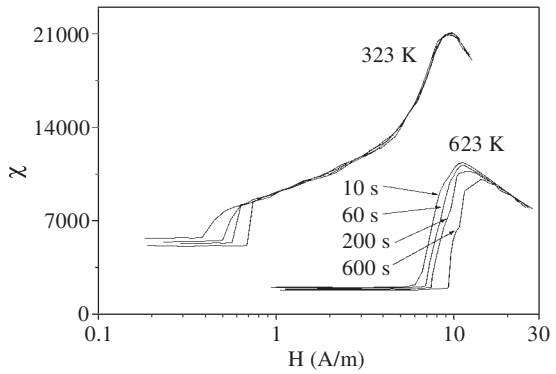

Figure 5. The field dependence of the susceptibility measured after demagnetization at marked temperatures with stabilization times $t_s = 10$, 30, 200 and 600 s.

the Nèel stabilization potential E_N. The Rayleigh potential is influenced by the type and space distribution of magnetically active defects, stresses and chemical inhomogeneities. The Nèel potential develops due to atom pair reorientation. The DW feels the superposition of these two potentials. The DW lies in the position of the E_R minimum after demagnetization. Atom pair axes reorientation processes form E_N, which deepens the DW potential well. A deeper and also steeper well decreases the DW mobility, which is macroscopically visible by the decrease of the initial susceptibility. Application of the external magnetic field pushes the DW from the equilibrium position. When the external field reaches a value equal to the DW pinning field, it irreversibly moves out from the potential well. Greater steepness of the well requires higher fields to push the DW out from the well. The maximum steepness is at the inflection point of the potential $\varphi_S = E_N + E_R$.

We have measured a set of $\chi(H)$-dependences in the temperature interval 323–623 K after $t_s = 10$, 60, 200 and 600 s stabilization. The stabilization time t_s is the waiting time between the end of the demagnetization and the start of the measurement. Typical $\chi(H)$ dependences can be seen in figure 5. The susceptibility increase for fields $H > H_{CR}$ is gradual at 323 K and takes place over a wide field range. It is given by a broad DW pinning field distribution [28]. χ abruptly increases in a narrow field region at 623 K, because the H_P are unified by the stabilization. From these dependences we constructed the time dependence of the critical fields at different temperatures. The time was calculated as the sum of the stabilization time and the measurement time up to critical field. All $H_{CR}(t)$ dependences have linear shape in logarithmic scale at the measured time interval; only their steepness changes with the temperature (figure 6). To have more comparable data, we estimated the critical field at 100 and 600 s after demagnetization. These are presented in figure 7. $H_{CR}(T)$ has inverse behaviour to $\chi(T)$, proving equation $H_{CR}(T)\chi(T) =$ constant. The time–temperature dependence of H_{CR} for binary alloys can be expressed as [29]

$$H_{CR}(t, T) = H_0(T) + \Delta H G(t, T), \tag{17}$$

where $H_0(T)$ is the unrelaxed critical field, given by the Rayleigh potential, and ΔH is the maximum change of H_{CR}. The data in figure 6 were fitted with the simple relation $H_{CR}(t) = H_0 + \Delta H \ln(t)$. We can subtract the contribution of the Rayleigh potential to the temperature dependence of H_{CR} by calculating the absolute change of H_{CR}, $\Delta H_{CR} = H_{CR}(600\text{ s}) - H_{CR}(100\text{ s})$. This dependence reflects only the temperature dependence of Nèel potential development between measuring times (figure 8). One can see two peaks in

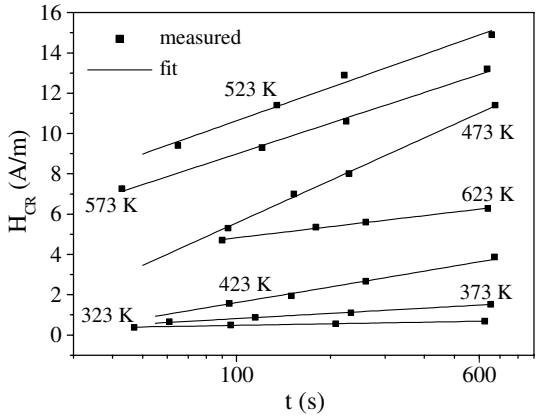

Figure 6. The time dependence of domain wall critical fields at marked temperatures.

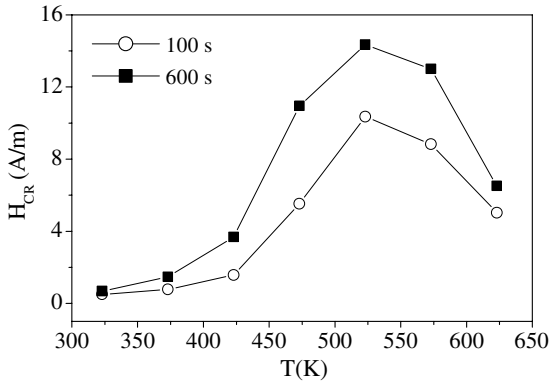

Figure 7. The temperature dependence of the domain wall critical field at $t_s = 100$ and 600 s after demagnetization.

the dependence. Each peak describes the contribution of different relaxation process to the formation of the Nèel potential, hence H_{CR} can be expressed as

$$H_{CR}(t,T) = H_0(T) + \Delta H^{(B)} G^{(B)}(t,T) + \Delta H^{(Si)} G^{(Si)}(t,T), \tag{18}$$

where the term $\Delta H^{(p)} G^{(p)}(t,T)$, $p =$ B or Si, characterizes the relaxation behaviour of pairs containing B and Si, respectively. The difference in peak positions when comparing with the reluctivity MAE spectrum is given by different times of measurements as well as the fact that the reluctivity after-effect is measured at small fields and the critical field after-effect at higher fields.

B-type relaxation intensively influences the H_{CR} values around 473 K. The contribution of Si-type relaxation to the formation of potential well steepness is smaller at these temperatures due to its large relaxation times. At temperatures around the second peak, B-type relaxation has short relaxation times; it deepens the potential well very quickly. The well formed by B-type relaxation is additionally deepened by Si-type relaxation, which has relaxation times comparable to the times of measurements. Superposition of these two effects forms the two-peak isochrone of ΔH_{CR}.

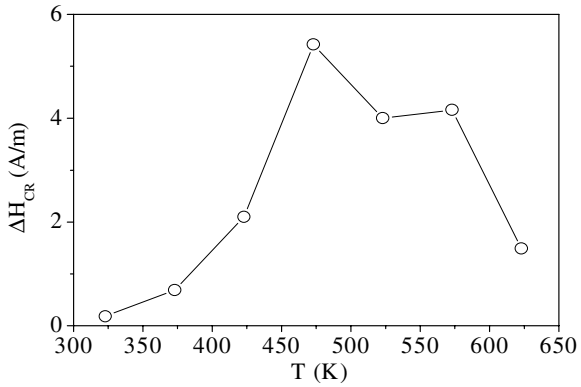

Figure 8. The isochrone of the critical field after-effect calculated from figure 7 as $\Delta H_{\mathrm{CR}} = H_{\mathrm{CR}}(600\ \mathrm{s}) - H_{\mathrm{CR}}(100\ \mathrm{s})$.

4. Conclusions

Directional ordering in amorphous $Co_{75}Si_{15}B_{10}$ alloys was investigated by means of magnetic after-effect spectroscopy and the Perminvar effect. An extended micromagnetic model was used for analysis of observed results. The model assumes different behaviours of atom pairs due to the different quantities $S^{(p)}$, $Q^{(p)}$, $\varepsilon_{i,j}^{(p)\mathrm{ex}}$, $\varepsilon_{i,j}^{(p)K}$ and $\varepsilon_{i,j}^{(p)\mathrm{el}}$. These parameters influence the activation parameters of directional reordering.

From the comparison of the MAE spectra of amorphous $Co_{75}Si_{15}B_{10}$ and $Co_{75}B_{25}$ alloys we identified two types of relaxations present in the $Co_{75}Si_{15}B_{10}$ sample. B-type relaxation originates from reorientations of Co–B atom pairs at temperatures around 383 K. Si-type relaxation originates from reorientations of Co–Si atom pairs at temperatures around 545 K. For a quantitative description of these processes we modified the micromagnetic model by introducing as many relaxation processes as a many metalloid elements sample contains. Each relaxation process has its own activation parameters. With the help of this model we found activation parameters for B-type relaxation $\tau_{0,\mathrm{AC}}^{(\mathrm{B})} = 7 \times 10^{-17}$ s and $Q_{\mathrm{AC}}^{*(\mathrm{B})} = 1.31$ eV. These values correlate very well with the activation parameters of the $Co_{75}B_{25}$ alloy, $\tau_{0,\mathrm{AC}} = 2 \times 10^{-17}$ s and $Q_{\mathrm{AC}}^{*} = 1.35$ eV. Si-type relaxation has activation parameters $\tau_{0,\mathrm{AC}}^{(\mathrm{Si})} = 6 \times 10^{-18}$ s and $Q_{\mathrm{AC}}^{*(\mathrm{Si})} = 1.96$ eV. After annealing the sample at 683 K for 30 min, the B-type relaxation peak shifts by 59 K and the Si-type relaxation peak by 31 K to higher temperature. The activation parameters change to values $\tau_{0,\mathrm{AN}}^{(\mathrm{B})} = 2 \times 10^{-15}$ s, $Q_{\mathrm{AN}}^{*(\mathrm{B})} = 1.38$ eV and $\tau_{0,\mathrm{AN}}^{(\mathrm{Si})} = 3 \times 10^{-17}$ s, $Q_{\mathrm{AN}}^{*(\mathrm{Si})} = 2.01$ eV.

Long-time isothermal measurements reflect the superposition of the two relaxation processes. The contributions of the particular relaxation processes were obtained by numerical analyses.

The MAE spectrum of the DW critical field has also two peaks. The impact of Co–B and Co–Si atom pair relaxation on the formation of the DW stabilization potential was discussed.

The results of different MR manifestations presented in this paper correlate very well, because they originate from the same atomic processes.

We have shown that directional ordering of different atom pairs takes place at different temperature ranges, and that the quantitative parameters characterizing the processes are also different. These differences should be taken into account in the analyses of all phenomena where directional ordering of atom pairs is of some importance.

Acknowledgment

This work was partly supported by Vega grant No 1/1017/04.

References

[1] Kronmüller H and Moser N 1983 *Amorphous Metallic Alloys* ed F E Luborsky (London: Butterworth) p 537
[2] Vojtanik P *et al* 1984 *J. Magn. Magn. Mater.* **41** 385
[3] Miyazaki T, Yang X and Takahashi M 1986 *J. Magn. Magn. Mater.* **59** 9
[4] Rettenmeier F, Kisdi-Koszo E and Kronmüller H 1986 *Phys. Status Solidi* a **93** 597
[5] Miyazaki T and Takahashi M 1985 *J. Appl. Phys.* **57** 3575
[6] Vojtanik P *et al* 1997 *Mater. Sci. Eng.* A **226** 736
[7] Varga R, Vojtanik P and Lovas A 1998 *J. Physique* IV **8** 63
[8] Varga R and Vojtanik P 1999 *J. Magn. Magn. Mater.* **197** 230
[9] Andrejco R *et al* 2004 *Phys. Status Solidi* a, at press
[10] Allia P and Vinai F 1982 *Phys. Rev.* B **26** 6141
[11] Xu R-F *et al* 1993 *Phys. Rev.* B **48** 15829
[12] Buttino G, Cecchetti A and Poppi M 2002 *J. Magn. Magn. Mater.* **241** 183
[13] Zbroszczyk J and Ciurzynska W 1997 *J. Phys.: Condens. Matter* **9** 4303
[14] Ciurzynska W, Haneczok G and Zbroszczyk J 1998 *J. Magn. Magn. Mater.* **189** 384
[15] Zhang Y Z, Dong C and Zhang D P 1985 *J. Magn. Magn. Mater.* **51** 75
[16] Rettenmeier F and Kronmüller H 1986 *Phys. Status Solidi* a **93** 221
[17] Kronmüller H *et al* 1984 *IEEE Trans. Magn.* **20** 1388
[18] Gawior W W 1994 *IEEE Trans. Magn.* **30** 507
[19] Kronmüller H 1983 *Phil. Mag.* B **48** 127
[20] Kronmüller H 1984 *J. Magn. Magn. Mater.* **41** 366
[21] Kronmüller H 1985 *Phys. Status Solidi* b **127** 531
[22] Miyazaki T and Takahashi M 1984 *J. Magn. Magn. Mater.* **42** 29
[23] Fujimori H *et al* 1977 *Amorphous Magnetism II* ed R A Levy and R Hasegawa (New York: Plenum) p 393
[24] Fdez-Gubieda M L *et al* 1996 *Phys. Rev.* B **53** 620
[25] Fdez-Gubieda M L *et al* 1997 *Europhys. Lett.* **40** 43
[26] Blythe H J 2002 *Phys. Status Solidi* a **181** 233
[27] Nèel L 1952 *J. Phys. Radium* **13** 249
[28] Varga R *et al* 2002 *Phys. Status Solidi* a **193** 103
[29] Vojtanik P *et al* 1994 *IEEE Trans. Magn.* **30** 476